UNIVERSITY OF TWENTE.

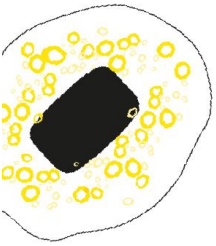

University of Twente

Active MR Tracking in a Static Phantom using a GRASP-sequence

Bachelor Thesis Biomedical Engineering

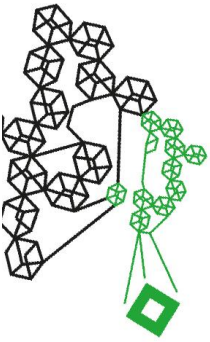

Committee:
dr.ir. Alic, L. (Chair)
dr.ir Brink, W.M. (Member)
dr. Dagnino, G. (Member)

Geurink, B.M.
29-6-2023

Abstract

Atrial fibrillation is the most prevalent cardiac arrhythmia with an increasing annual incidence. X-ray Fluoroscopy guided cardiac ablation is the current standard clinical intervention for treatment of atrial fibrillation. Recently, efforts have been made to introduce Magnetic Resonance Imaging (MRI)-guided ablations to improve the accuracy and reduce the relatively high recurrence rate associated with x-ray fluoroscopy ablations. MR-guidance could improve the procedure with 3D imaging while offering dynamic and physiological information .

This research investigates the potential of active device tracking using a GRASP-sequence. This sequence allows for anatomical imaging and device tracking from the same data set. Thus, directly accounting for bodily movements and, possibly, speeding up the procedure. The device tracking performance was tested in a static environment for seven positions in 3D space. An analysis of the performance was done based on the accuracy and precision of the measurements. In addition, the temporal resolution of device tracking was estimated and the dynamic tracking capabilities of GRASP have been shown.

The results show that the accuracy and precision of GRASP device tracking currently do not yet meet the requirements for clinical implementation. However, GRASP does offer potential and lays a foundation for future research on golden angle radial active device tracking. The flexibility of the sequence along with its ability to track dynamically provide opportunities for further exploration of this technique. Currently, the fairly low accuracy and precision of GRASP range up to, respectively, 16 and 8 millimetres. Also, the frame rate achieved with GRASP device tracking (2D: 6 fps / 3D: 1.85 fps) does not improve dynamic imaging compared to conventional methods.

Table of Contents

1. Introduction

Atrial Fibrillation (AF), the most prevalent form of cardiac arrhythmia, currently affects around 33 million individuals globally with a growing annual incidence of 5.4 million people [1]. Atrial Fibrillation develops when myocardial tissue induces unregulated electrical activity that replaces or supresses the normal cardiac cycle [2]. Treatment of AF amounts to an annual expense of 26 billion dollar in the United States alone [1].

Clinical intervention concerning AF typically involves cardiac ablation [1][3]. This procedure aims on impairing the cardiac tissue that causes the unregular electrical activity using an ablation catheter [3]. The main deficiency of cardiac ablations is the recurrence rate which is approximately 17 percent [1]. Ineffective ablations predominantly arise from inadequate visual guidance to steer the catheter to the right location and limited information on the extent of the lesion [4][5]. The intervention is guided through the current standard, X-ray fluoroscopy. A limitation of X-ray fluoroscopy is the fact that it only provides two dimensional imaging with poor contrast between soft tissues [4][5]. These two characteristics make it challenging for clinicians to guide the catheter towards the correct location. Despite this, the accuracy of the x-ray fluoroscopic catheter tracking itself is excellent with an average deviation of 0.64 millimetres with respect to the actual location while achieving a framerate of 17 frames per second, see Table 1 [6]. With X-ray fluoroscopy, catheter tracking is performed through small electrodes that are embedded in the catheter. The electrodes are distinguishable as a point of low intensity, the black dots along the body of the catheter as seen in Figure 1 [6]. These dots can be used for the determination of the location of the catheter. Most interventions make use of a single-plane system allowing for 2D anatomical imaging. Biplane x-ray fluoroscopy could be used to acquire 3D information but this modality is not used commonly as it is associated with high costs, longer procedures and higher exposure to ionizing radiation. Alternatively, another imaging modality like CT or MRI can be used to overlay a static 3D anatomical roadmap that improves the depiction of the surrounding anatomy. However, as the overlayed roadmap is static, respiratory motion needs to be accounted for as this could lead to tracking deviations of up to 14 mm [6]. This motion correction can be achieved through a Lasso or Coronal Sinus catheter, both visible in Figure 1. Thus, the complexity of the intervention mainly arises from the difficulty of guiding the catheter towards the right tissue due to the inability to adequately visualise the anatomy. This results in inaccuracy and high readmission rates. Also, it is important to note that continuous x-ray procedures expose the clinicians to undesired levels of ionizing radiation despite protective measures [4].

Table 1 Performance of x-ray fluoroscopic ablation catheter tracking displayed as the deviation (mm), success rate (%) and framerate (fps) of tracking [6].

	Tracking Performance
Deviation (mm)	0.64 ± 0.37
Success Rate (%)	99.2
Framerate (fps)	17

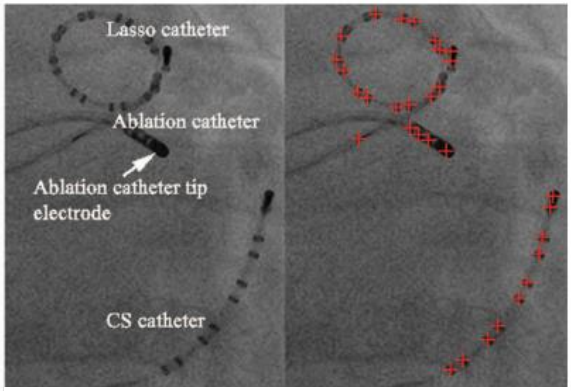

Figure 1 Visualization of x-ray fluoroscopic catheter tracking. The tracking of the electrodes in all three catheters is visualized by the red crosses. In addition to the ablation catheter, the Lasso and Coronal Sinus catheter that are used for respiratory motion correction are also shown [6].

In comparison to x-ray fluoroscopy, MR-guidance is able to provide high quality imaging of soft tissues, in three dimensions with a high spatial resolution, without the need for an overlayed roadmap. Using an overlayed roadmap is not optimal as it is time consuming and expensive to acquire the anatomical roadmap with another imaging modality before the ablation. In addition, correcting the movement

using a Lasso or Coronal Sinus catheter is suboptimal as not all bodily motion can be accounted for accurately because it is mainly aimed at correcting respiratory motion. Whereas with a MRI sequence that obtains both device tracking and anatomical imaging from the same dataset, all bodily motion could be accounted for directly. Additionally, MRI could offer the ability to depict physiologically relevant processes such as energy transfer to assess the extent of the lesion next to avoiding ionizing radiation [4][5]. The challenge of transforming cardiac ablation into an MRI-guided procedure lies in the fact that it is more difficult to combine catheter tracking and anatomical imaging up to a level that is adequate for clinical implementation. Due to the nature of 3D MRI acquisition physics, it is currently too time-intensive to acquire 3D anatomical imaging in combination with 3D tracking. This prevents implementation of real-time guidance. Another factor is the strong magnetic field in which the procedure is performed, requiring the use of MR-compatible equipment [5].

In order to facilitate adequate procedural guidance, an MRI-sequence needs to provide both real-time image acquisition and catheter tracking simultaneously. Catheter tracking with MRI can be classified as active or passive. During passive tracking, the catheter's position is determined through marker materials that are embedded in the catheter. The properties of the marker material induce local distortions in the image, e.g. image artifacts or signal voids, that can be tracked [4][7]. Active tracking, on the other hand, involves monitoring the catheter's position through MR-signals received by RF-coils that are embedded in the tip of the catheter [4][6]. An example of active MR tracking is shown in Figure 2. In this, an overlay of three pre-recorded anatomical planes is shown in which the location of the catheter is depicted as the intersection of the two coloured lines indicated by the yellow arrows [8]. This intersection identifies the signal that is obtained through the RF-coils in the tip of the catheter. It is important to note that Figure 2 is for illustrative purposes only as it does not demonstrate real-time acquisition of the anatomy.

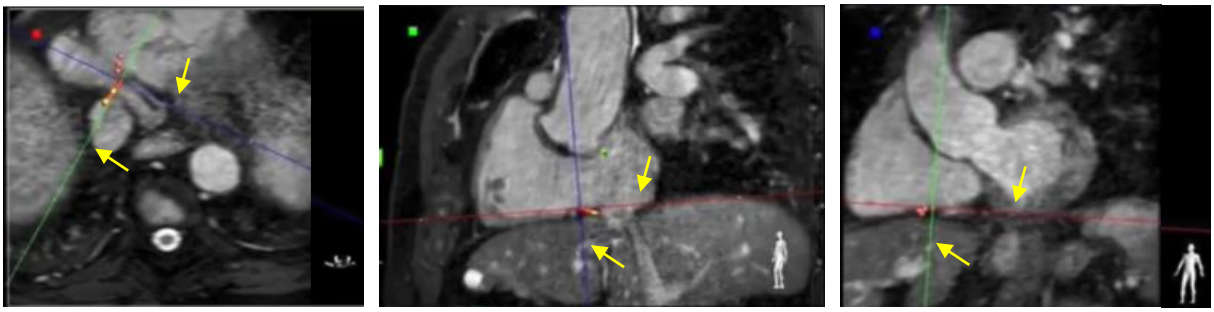

Figure 2 Representation of active MR-tracking. Important to note is the fact that the anatomical imaging is an overlay of pre-recorded acquisitions. In this, the catheter is localised through the intersection of the coloured lines indicated by the yellow arrows [8].

The main benefit of active tracking is the fact that it allows the image plane to be centred along the orientation of the catheter automatically. That is to say, the anatomical plane is automatically readjusted to depict the anatomy in which the catheter is located. This is possible as the signal obtained through the RF-coils provides quantitative information on the location of the catheter that can be used to readjust the anatomical plane [7]. In comparison, during passive tracking, the location of the catheter is determined visually based on artifacts in the image. Herein, no quantitative information regarding the location of the catheter is provided. Without this quantitative information, the anatomical plane cannot be readjusted automatically. Thus, when the catheter moves out of the anatomical plane, it has to be re-localised manually [7][9].

Generally, active MR-guided device tracking involves a real-time 2D image acquisition sequence, for instance a bSSFP sequence, that is interleaved with a dedicated tracking sequence [7]. The imaging geometry is often restricted to a 2D plane, as 3D imaging is too time-consuming. This technique achieves 3D active device tracking and 2D imaging at an acquisition speed of up to 10 frames per

second [7]. However, the tracking sequence may interfere with the steady-state magnetization that is build up during a bSSFP sequence, potentially causing artifacts in the anatomical image [10]. Moreover, the anatomical image can only be acquired in 2D. To address these limitations, the opportunities offered by other MRI sequences can be investigated. Key considerations in the search for a proper sequence are the ability to image in 3D, provide dynamic information and flexibility of tuning reconstruction parameters to optimize real-time reconstruction speed and quality. In addition, a sequence that is able to obtain both device tracking as well as anatomical imaging from the same dataset would eliminate the need for interleaving sequences, and avoid interference with steady-state magnetization that is build up during the sequence.

A sequence that addresses the aforementioned key considerations is the Golden-angle RAdial Sparse Parallel MRI (GRASP)-sequence. A GRASP-sequence could enable the user to obtain both MR device tracking and the construction of an anatomical image from the same dataset. GRASP combines Radial Golden-Angle (GA) acquisitions, Compressed Sensing and Parallel Imaging into a real-time acquisition sequence [11]. Out of these three techniques, the radial sampling of k-space according to the Golden Angle is the key principle on which the MR-device tracking examined in this study is based. A basic method for sampling k-space is a Cartesian path in which k-space is filled with horizontal or vertical lines. The principle of radial sampling relies on the lines being positioned radially in k-space like the spokes of a wheel. Addition of the GA assures that consecutive spokes are placed with a relative angle of 111.246 degrees, see Figure 3B. This ensures a highly uniform distribution of spokes through k-space. Benefits of this are an improved robustness with respect to motion and the possibility to undersample k-space. As k-space is sampled uniformly and each spoke samples the centre of k-space, a decrease in the number of spokes could reduce acquisition time without significantly compromising image quality [12]. Thus, with GRASP, it is easier to lower the number of spokes while maintaining a uniform k-space. Given that the number of lines through k-space can be reduced, hence speeding up the acquisition without significantly reducing the quality of the image, allows for real-time acquisitions.

The spoke wheel of radial acquired lines, sometimes referred to as a 'star', forms a 2D plane. Utilising a stack-of-stars k-space trajectory, the 2D GA radial sampled 'star' is shifted to three dimensional space by stacking several 2D 'stars' on top of each other. This is visualized in Figure 3 [13]. The stacked stars form the slice dimension along the z-direction (k_z). In this, the slices are acquired in a 'centric out' Cartesian order. That is to say, the order of slices is not set linearly from top to bottom but the first slice is acquired in the centre (k_z=0) with subsequent slices being placed towards the edges of k-space. The spokes in the xy-plane are sampled radially [12]. In GRASP, a specific spoke is acquired over all

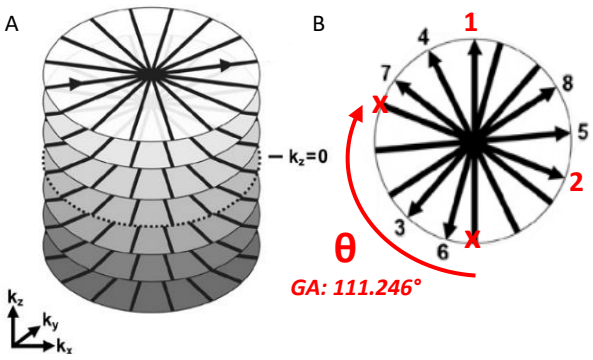

Figure 4 A) 3D Stack-of-Stars k-space trajectory with radial sampled stars in the (k_y,k_x)-plane stacked in the Cartesian sampled k_z-direction. B) Golden Angle spoke alignment in which the relative angular placement of consecutive spokes (e.g. 1-2) equals the GA = 111.246° [13].

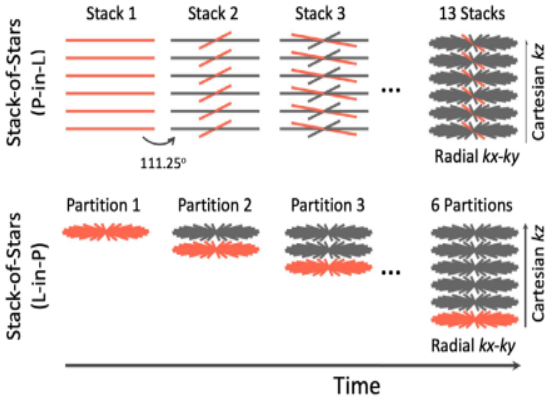

Figure 3 Radial P-in-L and L-in-P stack-of-stars ordering schemes. For P-in-L, all partitions are acquired first for each spoke before acquiring the next spoke. For L-in-P, all spokes in the x-y plane are acquired before sampling in the next partition [12].

slices (z) before acquiring the following spoke at another angular position. This method is also referred to as a 'Partition in Line' or 'P-in-L' stack-of-stars and allows for 3D localization as the position will be determined over all slices, see Figure 4 [12][13]. Stack-of-stars is often used because only a one-dimensional Fourier transform is required in the z-direction after which a stack of two-dimensional planes is obtained. Conversion to the two-dimensional plane eases the reconstruction.

In order to achieve the GA radial stack-of-stars ordering scheme the data is acquired through the pulse sequence shown in the diagram in Figure 5. A conventional 3D gradient-echo underlies this new GRASP-sequence [13]. The pulse sequence starts with an RF excitation pulse (a) initiated simultaneously with slab-selection through gradient (b). Gradient (c) rewinds the slab-selection and provides Cartesian phase-encoding in the slice direction while gradient (d) de-phases the READ-PHASE plane. ADC (f) collects the signal of readout gradient (e) followed by spoiling gradient (g) which ensures that residual magnetization along the axis is eliminated [13].

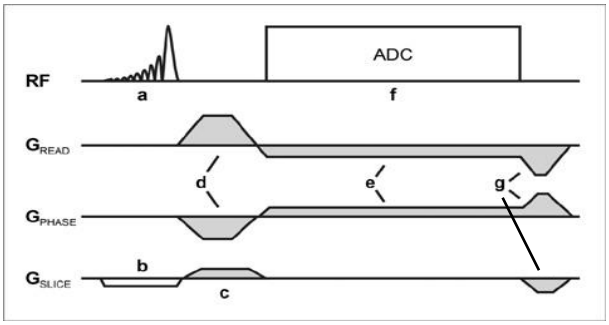

Figure 5 Sequence diagram of a GRASP-acquisition. G_{READ} representing the frequency-encoding gradients, G_{PHASE} representing the phase-encoding gradients and G_{SLICE} representing the slice-selection gradients. With A) RF pulse B) slab-selection gradient C) Slice Phase-encoding gradient D) dephasing of READ-PHASE plane E) Readout gradient F) ADC signal acquisition G) Spoiling gradient. [13]

GRASP has evolved over the years into a technique that provides improved high-quality real-time acquisitions [11]. However, the tracking capabilities of the GRASP sequence have not been assessed previously. In comparison to conventional techniques, GRASP may grant the ability to accelerate the acquisition due to the fact that it, potentially, could reconstruct both the anatomical image and the device tracking from the same data set eliminating the need for interleaving an imaging sequence with a tracking sequence. In addition, GRASP allows for three dimensional anatomical imaging where most conventional methods only grant two dimensional reconstruction.

The main focus of this research is to assess the active static device tracking capabilities of a GRASP-sequence. The question that arises is whether GRASP will improve the accuracy and precision of the localisation of the ablation catheter in comparison to conventional tracking methods like bSSFP-tracking. Considering that both components originate from the same dataset, anatomical movement such as cardiac motion and breathing can be directly accounted for. This research examines the active tracking performance of the GRASP sequence according to the following research question:

What level of accuracy and precision can be achieved using a GRASP sequence for active device tracking?

To assess the static tracking performance of the GRASP-sequence, the deviation from the catheter position in the experimental GRASP acquisition to the control acquisition will be a measure of GRASP's accuracy and precision. If GRASP proves to be useful, it could obtain better localisation of the ablation catheter while providing high-quality real-time acquisitions. Potentially speeding up the acquisition, achieving a higher framerate and enhanced guidance of the catheter during the intervention.

2. Methods

2.1 Experimental setup

To assess the performance of GRASP-localisation in a static environment, a static phantom was placed in a 1.5T MRI-scanner (Siemens Healthcare GmbH, Erlangen, Germany). The phantom, a simple plastic container, was filled with a paramagnetic solution of copper sulphate ($CuSO_4$) to reduce the T_1 and gain more signal. The MR-compatible Vision-MR Ablation Catheter (Imricor Medical Systems, Burnsville, United States) was inserted into the phantom and its position was varied in three dimensions throughout the experiment. The catheter was stabilized by guiding it over a cushion and fixating it with two sandbags, ensuring that the catheter tip would not lay on the bottom of the phantom. Thus, realizing a symmetric signal intensity around the tip of the catheter.

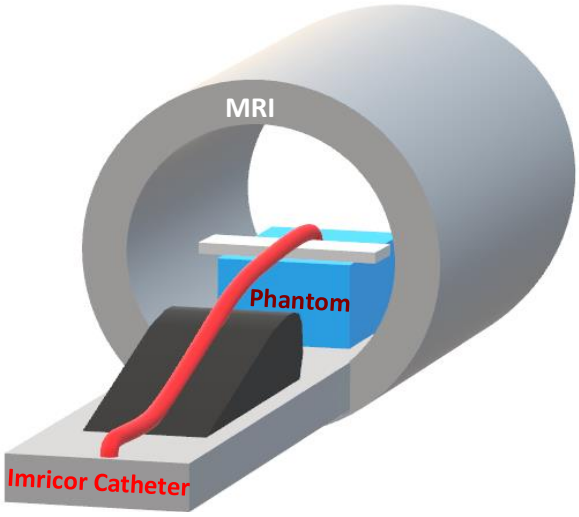

Figure 6 Visualization of the experimental setup. The phantom with the $CuSO_4$ solution was placed on the patient table. The catheter was guided over a cushion, hung in the phantom over a foam bar and fixed in position with two sandbags.

2.2 Experimental Protocol

In the experiment, the localisation performance of a control sequence was compared to the performance of the experimental GRASP-sequence. In this, the localisation by the conventional control sequence is assumed to be the golden standard so that the deviation of GRASP-localisation can be determined. The control sequence is the product sequence BEAT (Siemens Healthcare GmbH, Erlangen, Germany) that tracks the catheter's position in three dimensional space based on a spoiled gradient echo sequence [14]. For each BEAT localisation, three (X,Y,Z) one-dimensional orthogonal echoes are generated. The Fourier Transform of each echo results in a spatial profile with a signal peak that represents the proportional distance from the catheter to the isocentre of the scanner. The scanner automatically executes this protocol during the BEAT sequence and thus continuously determines the location of the catheter relative to the isocentre of the scanner.

The experimental positions of the catheter during the acquisitions were determined carefully. As visible in Figure 7, the catheter was positioned in seven positions, A up to G. These positions were selected to have variation in all three planes of the scanner. In addition, the decision was made to place the catheter as far as possible towards the extremities of the phantom to create large, easily noticeable, differences in the localisation coordinates. Positions A, B and C differ along the transverse (z) plane. Positions DBE differ along the sagittal (x) plane. Positions FBG differ along the coronal (y) plane. Considering these positions, the localisation performance along all three planes can be evaluated.

Both the BEAT and GRASP sequences were acquired for positions A up to G (Figure 7). After the static localisations, the dynamic tracking performance of GRASP was assessed in several acquisitions where the catheter was moved through the phantom by hand. A selection of sequence parameters are shown in Table 2. The comprehensive settings of the sequences used during this experiment are presented in Appendix A.

Table 2 Protocol settings for all sequences used.

Sequence	# Slices	FoV (mm)	Voxel (mm)	TE (ms)	TR (ms)	TA (s)
BEAT	1	360 x 360	2.8x2.8x10	1.46	225.12	0.3
GRASP	32	320 x 320	2.5x2.5x2.5	2.5	5.0	42.0

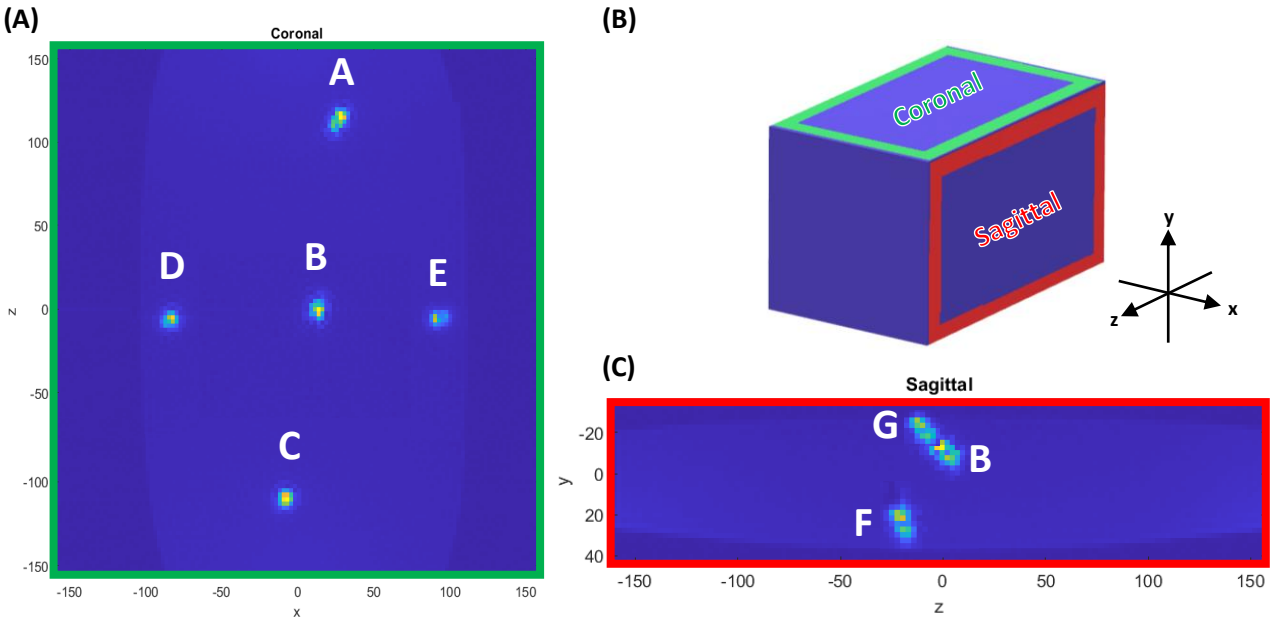

Figure 7 Visualization of the seven experimental catheter locations used during the experiment merged into one image. A) Coronal viewpoint showing the transverse differentiation for ABC and sagittal differentiation for DBE. B) Reference model of the phantom to visualize the planes and axis. C) Sagittal viewpoint showing the coronal differentiation for FBG

2.3 Post-Processing

Once the data was acquired, post-processing was done through MATLAB® (MathWorks, Natick Massachusetts, USA, version R2022a) with the raw data (.dat-files) obtained directly from the scanner. The script used for the analysis of the experimental data is provided in supplementary files. Some results obtained from the script were further processed in Excel (Microsoft, Redmond Washington, USA). The k-space data consists of 12 array elements and two catheter coils. These two coils are used to locate the catheter which is done using a MATLAB script. The other 12 coils are used to acquire an anatomical DICOM images of the phantom, like the ones visible in Figure 5AC.

In order to locate the catheter, the k-space data was extracted from the .dat files through the MapVBVD function. This function reads and organises the raw twix data obtained from the scanner. After this, it was Fourier transformed in the third dimension (k_z) followed by a Fourier transform in the first dimension. Before further processing of the data, it must be determined which of the, in this case, 14 channels contain the data of the two catheter coils. A plot was made for all channels from which the catheter coils can be differentiated easily through their different signal characteristics. The two previously conducted Fourier transformations result in spatial projections showing a signal peak indicating the catheter location. By determining the spatial profiles for all partitions, the location of the catheter in the slice-axis (y) can be identified. The partition with the highest signal peak depicts the catheter location on the y-axis (Figure 8). This determination results in a slice number in which the catheter is most likely located. This is necessary for further processing as the localisation in the xz-

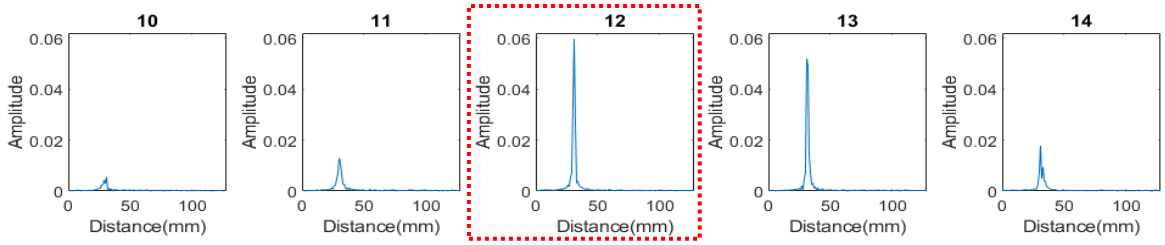

Figure 8 Spatial profiles of slices 10-15 for one line. In this case, the catheter is located in slice 12 as the highest peak is given for this partition. The further the slice is from the location of the catheter the lower the signal peak.

plane needs to be done for a specific slice number. For better approximation of the actual y-position, the weighted average slice location ($\hat{y}$) with respect to intensities over all partitions is determined according to the 'centre of mass' determination given Equation 1 for *n* number of slices. The sum of all slice-intensities ($Intensity_i$) for slices (i) times the slice-number (y_i) is divided by the sum of all slice-intensities ($Intensity_i$).

$$\hat{y} = \frac{\sum_{i=1}^{n} Intensity_i * y_i}{\sum_{i=1}^{n} Intensity_i} \quad (1)$$

Now the catheter is located on the y-axis, the remaining two dimensions can be determined based on the projections of two spokes acquired in the partition with the highest signal. A 2D inverse Radon Transform of these projections at their relative angles provides a magnitude image in which the intersection of both projections indicates the catheter's position in the xz-plane (Figure 7D). For this, the relative angular placement of the two spokes in the radial trajectory needs to be determined first.

A golden angle trajectory is based on the golden ratio (GR). A certain ratio A:B is equal to the golden ratio if the equations in Equation 2 hold. Solving the equations given in Equation 2 yields the golden ratio that equals 1.618, Equation 3 [12]. In this research, full-spoke golden-angle radial sampling is used which means that spokes only need to be acquired for half a circle (180°) to sample all of k-space [12]. This grants the golden ratio of approximately 111.246 according to Equation 4.

$$GR = \frac{a+b}{a} = \frac{a}{b} = \frac{1+b}{a} \quad (2) \qquad GR = \frac{1+\sqrt{5}}{2} \approx 1.618 \quad (3) \qquad GA = \frac{180}{GR} \approx 111.246 \quad (4)\ [12]$$

For any number of consecutive acquisitions, the spokes are distributed uniformly through k-space due to the golden angle radial sampling. It is necessary to know the angular placements of the spokes in k-space to be able to reconstruct a magnitude map of two spokes at their relative angle. In this sequence, the first spoke was placed at an angle of minus 90 degrees (270°). Subsequent spokes are placed according to the golden ratio with increments of 111.246°. To set up an array with the relative angular positions of each spoke, Equation 5 is used. For spokes 1 to *n*, its angular position is determined using the modulo operator. The modulo operator determines what remains after division of element A by element B (Equation 5) [12]. Thus, placing the first spoke at minus 90 degrees as mod(0,360) = 0. Using Equation 6, an array of relative angles between the spokes was set up for n spokes.

$$-90 + mod(A, B) \quad (5) \qquad -90 + mod\left(\frac{180}{GR} * (n-1), 360\right) \quad (6)\ [12]$$

For full-spoke golden-angle radial sampling, the Cartesian signal equation has to be rewritten to fit the polar scheme in which the spokes are acquired. Thus, the equations for x and y in Equation 7 that transform Cartesian to Polar coordinates need to be implemented in the Cartesian signal equation s(x,y). Then, a 2D Fourier transform of k-space $F(k_x,k_y)$ or $F(k_r,k_\theta)$ with parameters k_x, k_y, k_r and k_θ which are the Fourier conjugates of, respectively, x ,y, r and θ is performed [15]. This results in the polar signal equation given in Equation 8 that describes k-space for angular placement of spokes along angle θ with r being the position along the spoke relative to k_0.

$$x = rcos\theta \quad y = rsin\theta \;\rightarrow\; s(x,y) = \int_{-\infty}^{+\infty}\int_{-\infty}^{+\infty} F(k_x,k_y)e^{2\pi i[k_x x + k_y y]}dxdy \quad (7)\ [15]$$

$$s(r,\theta) = \int_{k_\theta=0}^{2\pi}\int_{k_r=0}^{\infty} F(k_r,k_\theta)e^{2\pi i r k_r \cos(k_\theta-\theta)}\, k_r dk_r dk_\theta \quad (8)\ [15]$$

Then, for two consecutive spokes, a projection can be obtained from k-space using a 1-dimensional Fourier transform (FT), Figure 9AB. These projections show a spatial profile with a signal peak that represents the location of the catheter. A radon transform of these projections will provide a magnitude map with the location of the catheter given as a high intensity spot (Figure 7D). Using this method, the location of the catheter can be determined faster as only two spokes are required to obtain a localisation. In contrast, localisation of the catheter through obtaining the entire image requires all spokes which is more time consuming.

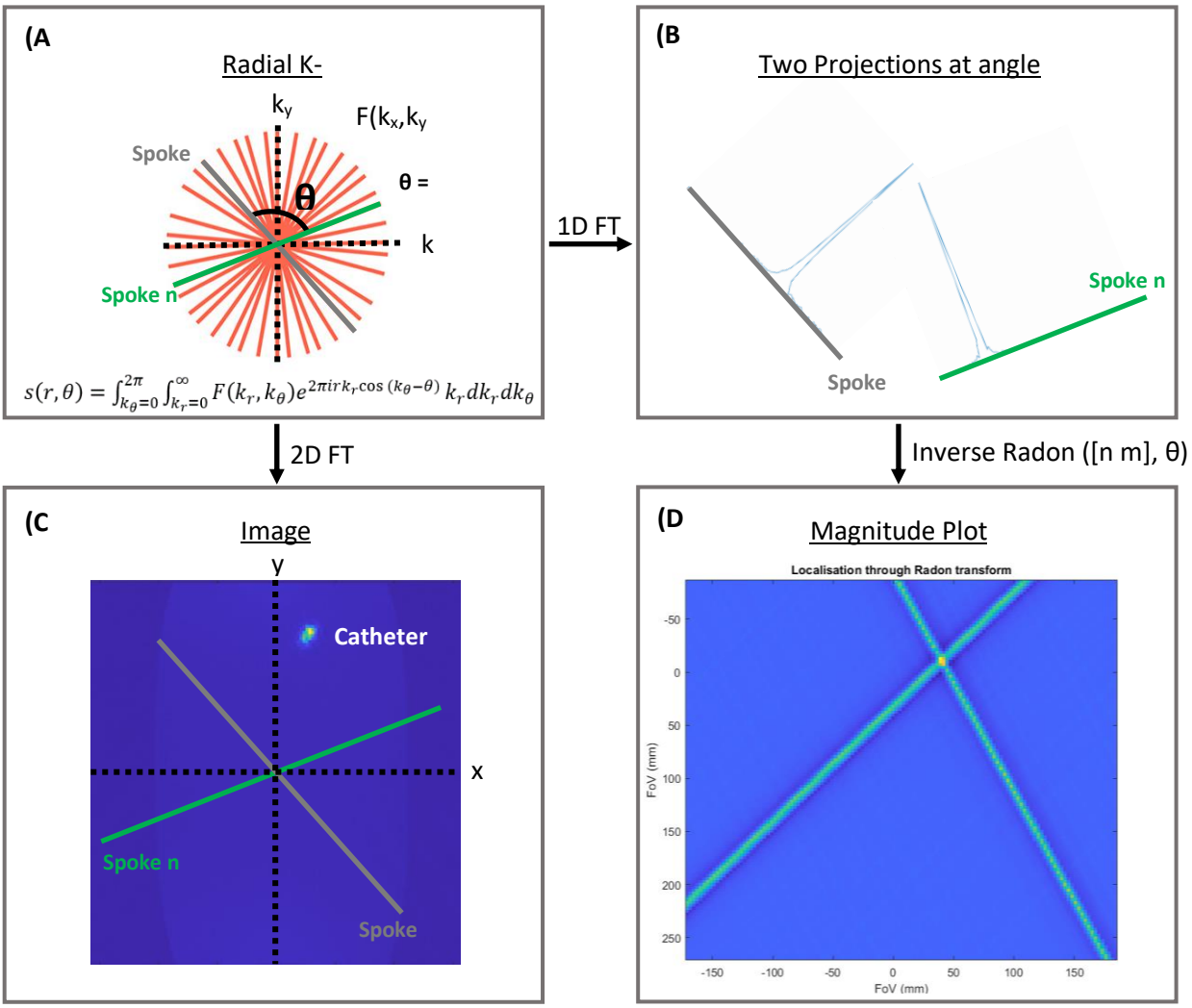

Figure 9 Flowchart of calculations to achieve a magnitude map. A) Radial k-space with two spokes with a relative angle equal to the GA (111.246°). Underneath is the signal equation for a radial acquisition shown. B) The spatial projections of each spoke at their relative angular placement obtained through a 1D Fourier transform (FT). They show a signal peak that represents the location of the catheter. C) Image that is obtained through a 2D FT that shows the actual coil location. D) Magnitude plot that is obtained through a Radon transform of both projections at the relative angle theta. The intensity peak at the intersectoin represents the location of the catheter in the xy-plane.

2.4 Localisation Performance

To draw a conclusion on the performance of active device tracking through a GRASP sequence, the meaning of 'performance' must first be established. Performance is defined with two distinct measures. Namely, accuracy and precision of the GRASP-localisations. Accuracy is the extent to which the measurements actually show the correct location, how close are measurements to the correct location. Precision shows the inter-variability of the measurements.

2.4.1 Accuracy

Both the experimental sequence and the control sequence will locate the catheter in three dimensional space (x,y,z). Based on the coordinates of the two localisations the Euclidian distance between these points can be determined using Equation 9 [16].

$$Euclidian\ Distance = \sqrt{(x_2 - x_1)^2 + (y_2 - y_1)^2 + (z_2 - z_1)^2} \quad (9)\ [16]$$

This distance, the Euclidian deviation of the two localisations, will be a measurement for the accuracy of the GRASP-sequence. This determination of accuracy is performed twice. First, the experimental GRASP-sequence is compared with the control sequence BEAT. BEAT specifies one (x,y,z) coordinate for each catheter coil whereas with GRASP, a coordinate can be obtained for each arbitrary combination of two consecutive spokes. To assess the accuracy of GRASP, the mean location along all axis was calculated for all combinations of two spokes which resulted in one (x,y,z) coordinate per catheter coil. Using the three-dimensional BEAT and averaged GRASP coordinates, the Euclidian distance was calculated through Equation 9.

Second, a comparison is made between the GRASP localisation of the catheter coils and the DICOM images that are obtained through the array coils with the same GRASP-sequence. The DICOM depicts the phantom with the catheter that looks like a roundish structure with a higher intensity, as visible in Figure 9C. These images and the corresponding position of the intensity peak were obtained through a MATLAB script. The DICOM shows only one intensity peak instead of the expected two peaks, one per coil. Across all experimental positions, it varies which of the two coils matches the position determined by DICOM the best. Consequently, it was not possible to determine whether the DICOMs showed one specific coil or averaged the intensity over both coils. Therefore, it was chosen to average over both coils to approximate the location most closely. Thus, the GRASP data of both coils was averaged, for comparison with the DICOM images. This results in a single (x,y,z) coordinate for both GRASP and DICOM over which the Euclidean distance can be determined (Equation 9).

2.4.2 Precision

GRASP is able to localize the catheter based on two consecutive spokes. To quantify precision, the mean deviation of all localisations based on two spokes will be compared to the joint average position. That is to say, an array of all x-positions is set up. The average x-position is subtracted from all entries in this array. Then, all entries are modified to their absolute value after which the array is averaged, resulting in the precision for the x-axis. This is done according to Equation 9.

$$Precision_x = mean(abs(x_i - mean(x)) \quad (9)$$

Another measure that is used to quantify the precision of measurements is a Root Mean Square Error (RMSE) determination [16]. This is calculated according to Equation 10 for n number of positions. All individual deviations (D_i) from the joint average position are determined after which the Root Mean Square Error of these deviations is taken [16].

$$D_i = x_i - \frac{1}{n}\sum_{i=1}^{n} x_i \qquad Precision_x = \sqrt{\frac{\sum_{i=1}^{n}(D_i)^2}{n}} \quad (10)\ [16]$$

3. Results

This experiment focused on establishing the accuracy and precision of active static device tracking using a GRASP sequence. In succession of the acquisitions described in the method, the results were obtained during post-processing based on the collected raw data. In addition to the accuracy and precision, the temporal resolution of the acquisition and reconstruction are determined and dynamic tracking capabilities are shown.

3.1 Accuracy

Figure 10 plots the accuracy of the experimental method, GRASP, in comparison to the control variables BEAT and DICOM for each location. The bars represent the Euclidian Deviation in millimetres from the mean GRASP localisation to BEAT- and DICOM-localisations. This deviation is given for both coils in the comparison between GRASP and BEAT as both methods grant an (x,y,z)-coordinate for both coils. A DICOM-image does not show both distinct coils, thus, the mean of both coils determined by GRASP is compared to the DICOM-localisation.

The accuracy is shown for all seven experimental positions. It is easy to notice that in all situations the GRASP-localisation deviates from the control variables. The accuracy between the control variables is reasonably equivalent for most positions, with the exception of a some measurements such as position D DICOM, F BEAT Coil 1. Position G overall shows a significant deviation and substantial differences among the control variables. One notable observation is that the accuracy for positions B,F,G are considerably lower compared to the other positions. The average deviation per control variable over all positions is given in table 3. Table 3 also shows the average deviation per position over all control variables. It is noticeable that DICOM in general deviates a bit more in comparison to BEAT. It is also worth noting that that positions F and G in particular, have an exceptionally large deviation when compared to the other positions.

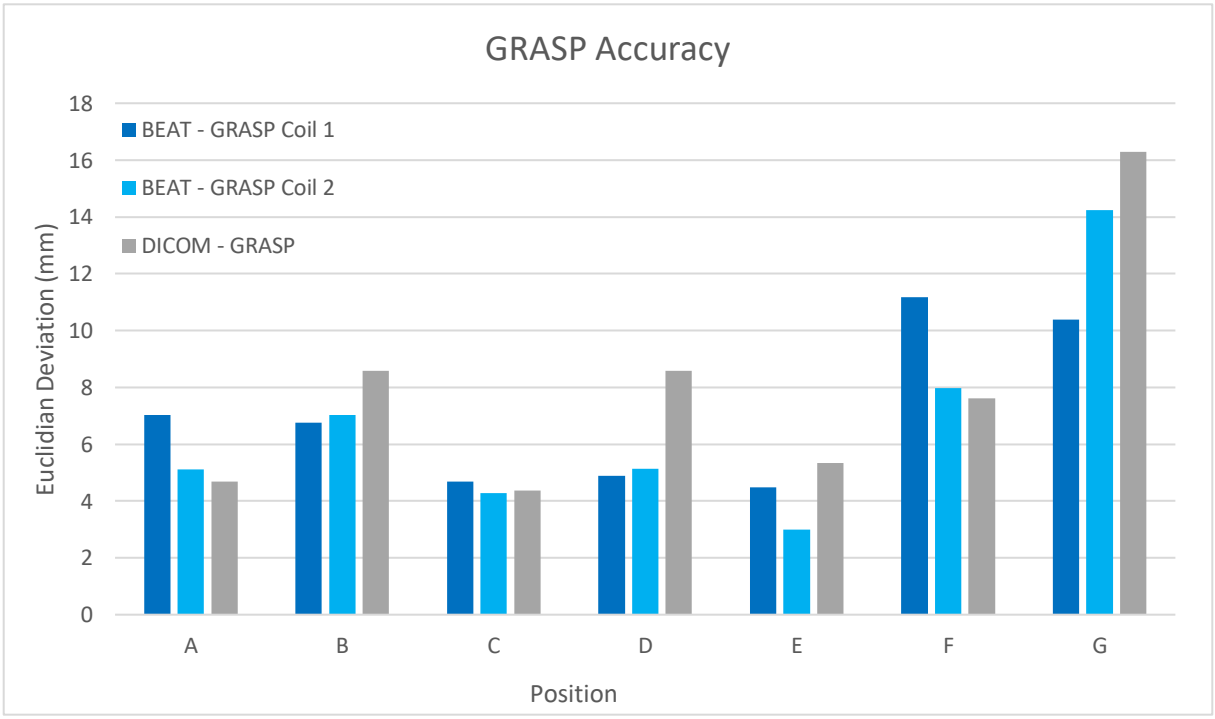

Figure 10 Graph of GRASP accuracy in comparison to control variables BEAT and DICOM. The graph shows the Euclidian Deviation in millimetres from the experimental GRASP localisation to the control localisations.

Table 3 Mean deviation of GRASP to the control in millimetres for all control variables and positions.

	Error BEAT - GRASP C1	Error BEAT - GRASP C2	Error DICOM - GRASP
Mean deviation (mm)	7.1	6.7	7.9

	A	B	C	D	E	F	G
Mean deviation (mm)	5.6	7.5	4.4	6.2	4.3	8.9	13.6

To better understand the mean Euclidian deviations (GRASP-BEAT) shown in Figure 10, the individual localisations of spoke pairs 100 till 150 were plotted sequentially in Figure 11. In these plots, it is easily noticeable that the GRASP localisations show a sawtooth pattern. Thus, the position determinations through GRASP do not show a uniform value like the BEAT-localisations, but rather a fluctuating pattern. It is also noticeable that the average of these GRASP localisations does not match the position determined by BEAT. The average sagittal (x) GRASP location is, for both positions, lower than the BEAT location. A similar situation occurs for the transverse plane (z) where the average GRASP location exceeds the BEAT determination for both positions.

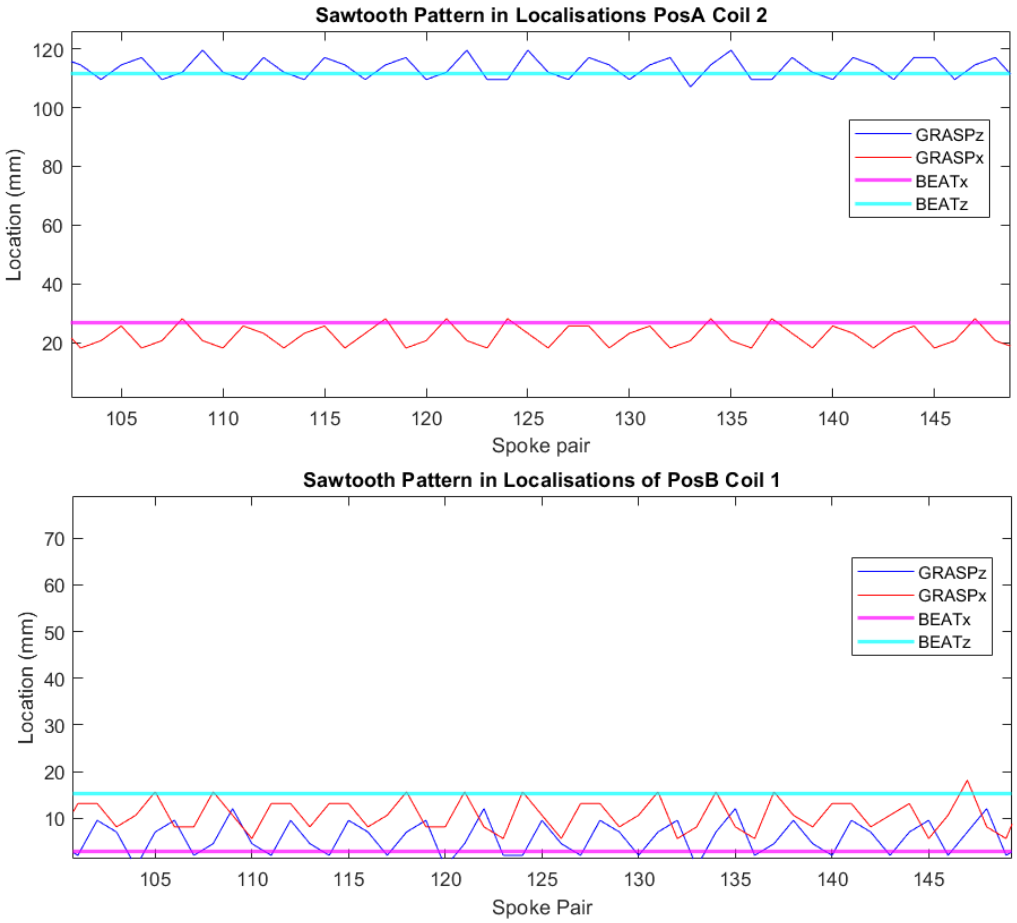

Figure 11 Visualization of individual localisations [100 150] for Position A Coil 2 and Position B Coil 1. The dark blue and red line represent the GRASP measurements for the corresponding spoke pair. A sawtooth pattern is clearly noticeable in these localisations. The magenta and cyan line show the corresponding BEAT location.

3.2 Precision

Figure 12 plots the precision of GRASP. This is established as the mean deviation from all spoke-pair localisations to the joint average localisation. The bars in Figure 10 show this mean deviation from the joint average per coil for the sagittal (x) and transverse (z) plane. The error bars show the maximal deviation from one of the spoke-pair localisations to the mean deviation. That is to say, for position A coil 1, the mean deviation from the joint average is 3.2 millimetre. However, there is at least one spoke-pair that deviates to a maximum of 7.5 millimetre from the joint average. It is clearly visible that all localisations have a reasonable deviation at approximately three millimetres. In addition, it is worth noting that the maximal deviations from the joint average indicated by the error bars are quite large. The maximal deviation consists of more than twice the mean deviation in 9 out of 14 positions. There is no clear difference in the precision of localisation between the transverse, sagittal and coronal planes.

The RMSE Precision assessment in Figure 13 yields a precision that is almost equal to the precision that results from the first calculation. For all locations, the RMSE Precision is less than the other precision determination as RMSE mean deviation from the joint average is slightly higher. Again, it is noticeable that the precision is fairly equal across all positions and coils. There are no major anomalies.

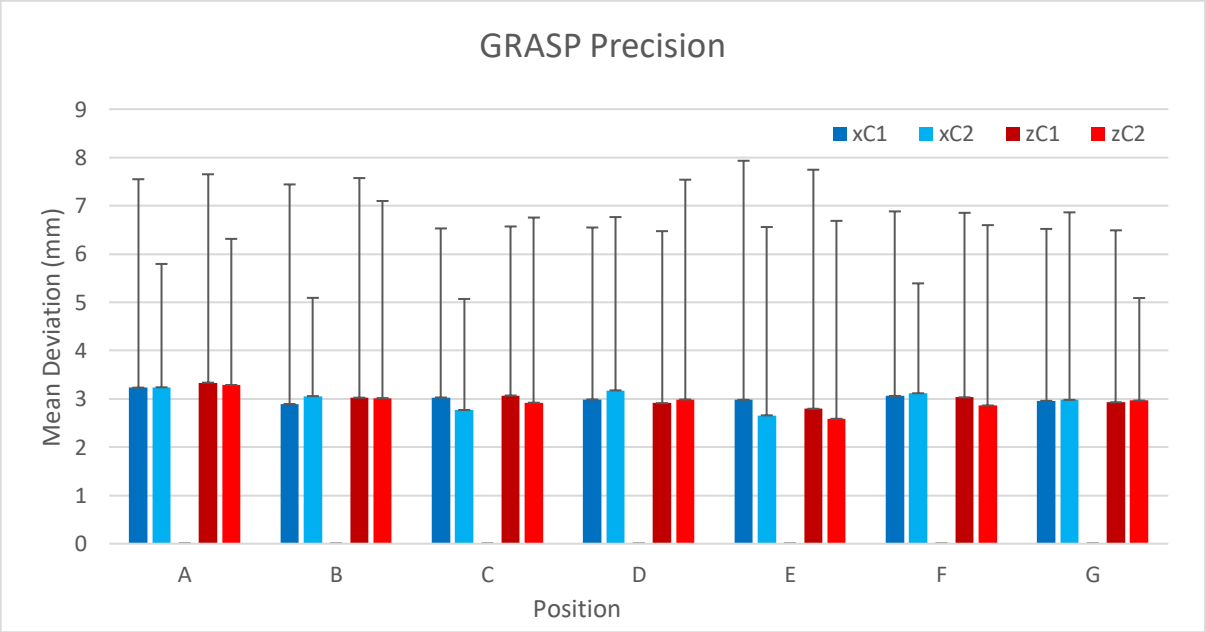

Figure 6 Graph of GRASP Precision. The graph shows the mean deviation from the joint average in millimetres with the errors bars as maximal deviation from the joint average in millimetres. This is visualized for each position A to G for planes x and z and coils C1 and C2.

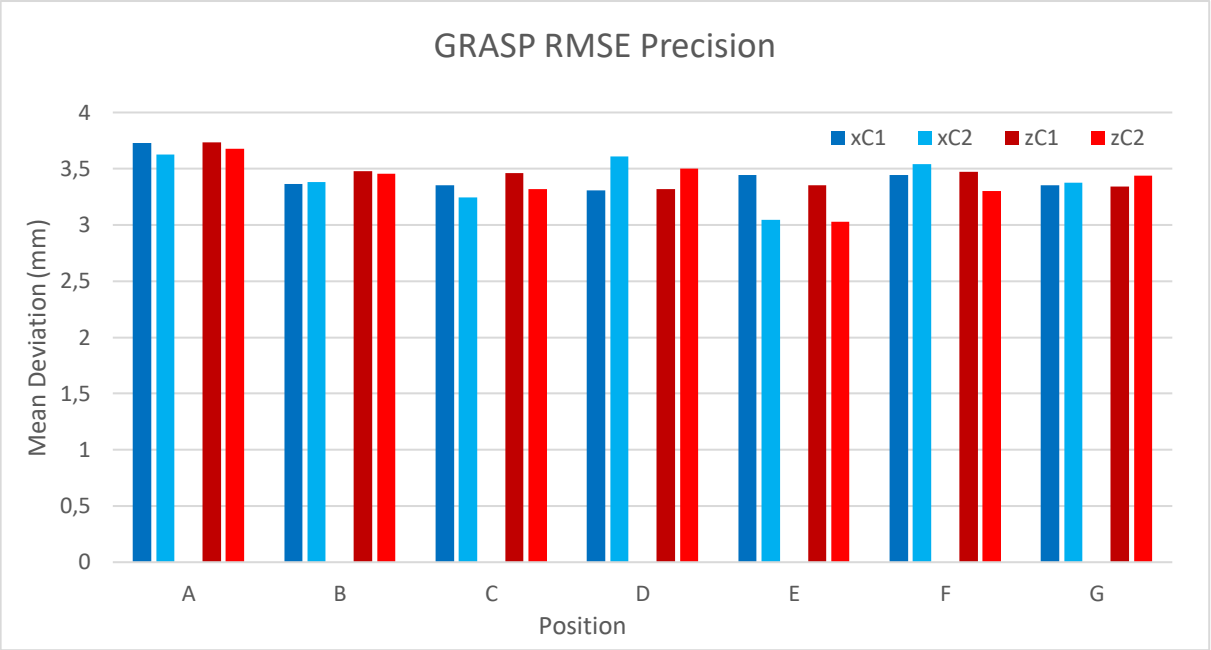

Figure 7 Graph of GRASP RMSE Precision. The graph shows the mean deviation from the joint average in millimetres for each position A to G for planes x and z and coils C1 and C2.

3.3 Tracking speed

The required time for the localisation of the catheter depends on the whether it must be determined in two- or three-dimensions. For the localisation of the catheter in a 2D plane, acquiring two spokes is enough to be able to determine the position of the catheter. However, following the Partition in Line method that GRASP uses, for 3D localisation, 64 spokes need to be acquired as all spokes at a certain angular position get acquired for 32 partitions first, before the next spoke is acquired for 32 partitions. Thus, according to Equation 11 for the acquisition time. The time to track the catheter in two dimensional space amounts to the repetition time (5 milliseconds) times the number of spokes (*n*) in the $Phase_x$-direction, in this case 10 milliseconds. To acquire a 3D localisation the phase-encoding steps in the slice direction (y) need to be accounted for. This amounts to an acquisition time of 640 milliseconds.

$$Acquisition\ time\ \approx T_R * Phase_x(n) * Phase_y \quad (11)$$

The reconstruction of the (x,y,z)-localisations were performed and timed through MATLAB. The localisation is done in the 2D xz-plane and in the slice (y) plane to acquire a third dimension. These are separate reconstructions as not each 2D localisation needs an update of the third (slice) dimension. Reconstruction times were measured using the tic-toc MATLAB command and came down to approximately 170 milliseconds for the xz-plane and 540 milliseconds for the slice dimension. The achievable frame rate is dependent on the times mentioned above. In the determination of a 2D location, the limiting factor is the reconstruction time. Therefore, the framerate amounts to approximately 5.9 (1/0.17) frames per second. When determining a 3D location, the reconstruction time again limits the framerate which consequently amounts to, roughly, 1.85 (1/0.54) frames per second. A summary of all the beforementioned times is given in Table 4.

	Acquisition Time (ms)	**Reconstruction Time (ms)**	**Framerate (fps)**
2D	10	170	5.9
3D	320	540	1.85

Table 4 Summary of acquisition and reconstruction times with their respective framerate for 2D and 3D tracking.

3.4 Dynamic Tracking

In addition to the accuracy and precision measurements of static GRASP-tracking, an attempt was made to show the active dynamic tracking capabilities of the GRASP sequence. For this, the catheter was moved through the phantom and different patterns were ‘drawn’. To visualize the active tracking capabilities a line along the transverse plane and the letters ‘UT’ were drawn in the phantom. This is shown in Figure 14. Each dot represents a localisation by two consecutive spokes through a radon transform. When visualizing a video of all localisations after one another, a magnitude plot for each localisation is shown and a dot is placed on the point with the maximum intensity. The placement of all consecutive dots forms the shapes in Figure 14. The transverse line is clearly visible with the most dots placed at the end point of the lines. The amount of dots in a certain region expresses the amount of localisations that have been done in that region and, thus, the time the catheter has been in this region. For the drawn letters, it is easy to notice that there is a lot more noise as a lot of dot are placed randomly throughout the field of view, Figure 14B. However, the letters themselves are still distinguishable. After setting up a threshold to eliminate noise localisations, the letters themselves are clearly visible, Figure 14C.

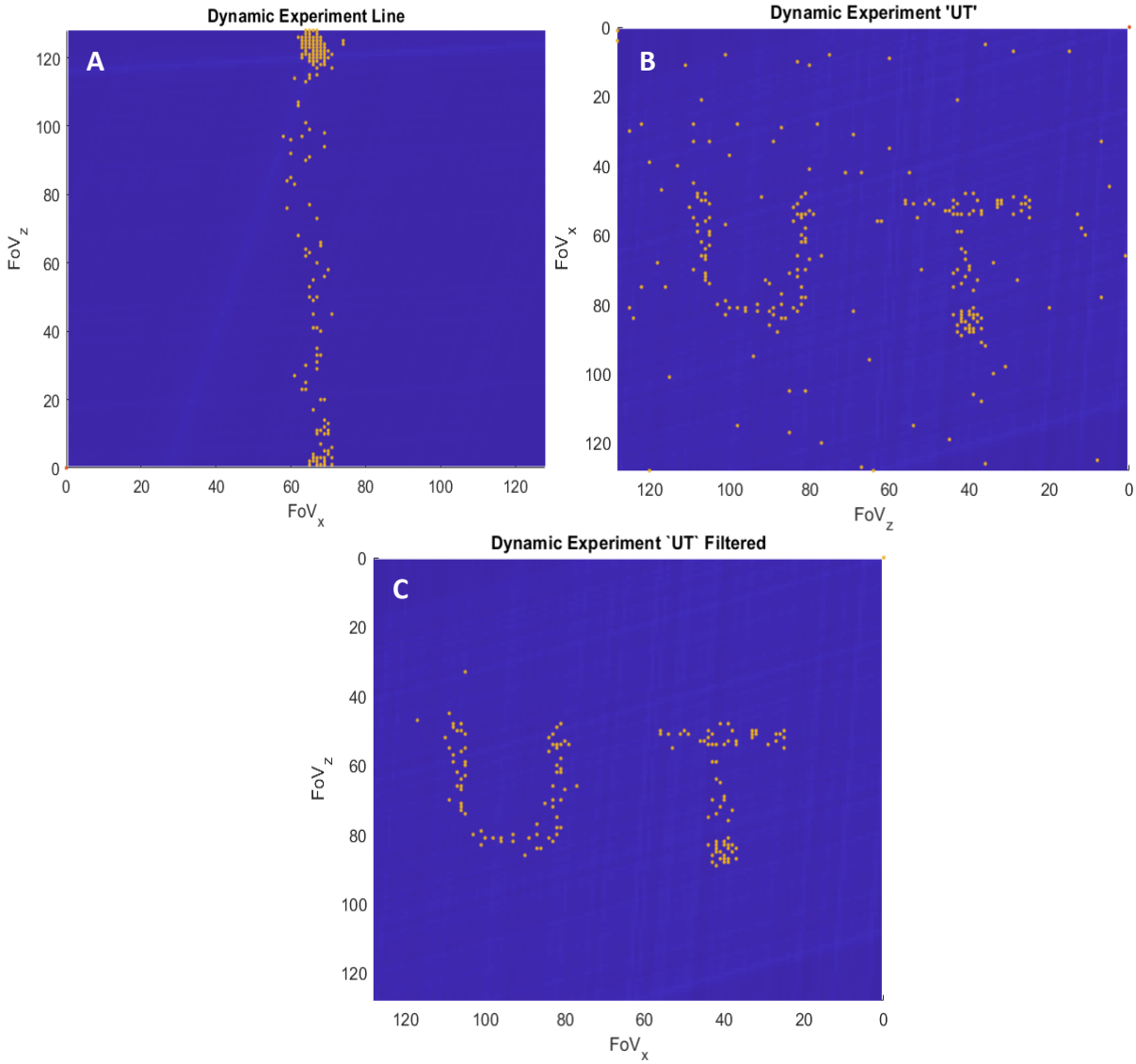

Figure 8 Graphs of dynamic GRASP tracking for a line in the transverse plane (A) and the letters 'UT' (B). The letters were flipped and rotated to present them according to the reading direction. C) shows the letters UT with a signal threshold for plotting the dots to remove noise.

4. Discussion

The main goal of this research was to investigate the active device tracking performance of a GRASP-sequence in a static environment. In this, the term 'performance' is defined through a accuracy and precision measurement. The experimental setup consisted of a static phantom in which, for several locations along the three planes, the accuracy and precision was determined. The accuracy of the GRASP sequence was established with respect to the Siemens BEAT sequence and the DICOM images that were obtained from the same GRASP dataset as the GRASP-tracking. For the precision, the mean deviation from the joint average location was determined alongside an RMSE assessment.

With regards to accuracy measurements, there is a reasonable deviation between the GRASP-localisations in comparison to the control variables BEAT and DICOM. Average deviations of GRASP with respect to BEAT amounting to 7.1 millimetres and 6.7 millimetres for coils one and two. When compared with DICOM, GRASP deviates 7.9 mm on average. In general, the GRASP accuracy measurements for the two coils are fairly equivalent with a few exceptions. Especially for positions F and G, the two coils differ significantly in both measurements. The difference across the control variables could be explained by some deviant measurements that increase the DICOM mean. In addition, the result for the two GRASP coils is averaged in order to be able to compare it with DICOM. This potentially misrepresents the actual situation.

The oscillating localizations (sawtooth) by GRASP are a possible cause for the anomalies between the experimental and control variables. GRASP is unable to facilitate unambiguous localizations as the determined positions fluctuate. However, since this oscillation is more or less systematic over both planes (x,z) and over all positions, there might be a way to correct this systematic error. Essentially, the oscillating pattern means that the positioned spokes do not move exactly through k_0 but have a small deviation. This misalignment of spokes in k-space could be due to incorrect calibrated gradients or eddy currents. When all the spokes will be correctly positioned through k0, the oscillating pattern may vanish. Other than the potential cause that was just mentioned, the deviation between the measurements can also be caused by arbitrary errors. To address this issue, it would be better to perform the accuracy measurements, at least, in triplet for each position in the phantom. This allows for averaging, eliminating arbitrary measurement errors. Consequently, a more unambiguous conclusion can be drawn regarding the accuracy of GRASP tracking.

The precision analysis shows a fairly uniform result. For both methods, the individual values per coil and plane correspond reasonably well. The mean deviation of the joint average yields an average precision of 3.0 millimetres. The RMSE determination shows a mean precision of 3.4 millimetres. Important to note is the deviation of individual measurements with regards to the previous mentioned averaged precision values. The maximal deviation of an individual spoke pair relative to the joint average was calculated to be 7.9 millimetres. Given that the values for precision are fairly even across both methods, there is no reason to question the correctness of the precision value in this specific set of measurements. However, the aforementioned oscillating pattern that occurs in the GRASP localizations also interferes with the precision value. The fluctuations create a larger deviation to the joint average in comparison to the scenario in which the GRASP positions would follow a relatively straight line. This results in a poorer precision value.

In the valuation of accuracy and precision, it must be taken into account that this experiment took place in a highly simplified environment. Factors that could have affected these two measures have been minimised. The experiment takes place in a static phantom with a static catheter. A paramagnetic solution was also used to shorten the T1 time. In a clinical situation, both the phantom and the catheter will not be static. The phantom would be subject to bodily movements such as heart rate and breathing

as well as blood flow. Similarly, the catheter would move through the body instead of being static. These are all factors that indicate that GRASP accuracy and precision tested in a clinically relevant situation will, most likely, be worse than the current values.

A comparison of the obtained results with the current gold standard for catheter tracking, x-ray fluoroscopy, shows that there is a significant deviation between the accuracy of GRASP tracking and the accuracy of x-ray fluoroscopic tracking. With GRASP an average accuracy of 7.2 millimetres was achieved. This is more than 10 times lower than the accuracy that can be achieved with x-ray fluoroscopy, on average 0.64 millimetres [6].

The acquisition times for 2D and 3D localisation were determined to amount to 10 and 320 milliseconds. Reconstruction of the location with the MATLAB script amounted to approximately 170 milliseconds for a 2D location and 540 milliseconds for a 3D location. The reconstruction time is also highly dependent on the computing power of the hardware on which the script is run, possibly allowing for a faster reconstruction when providing more computational power. GRASP's stack-of-stars trajectory is probably significantly slower in comparison to e.g. a 3D koosh ball trajectory in which three arbitrary orthogonal lines could be sufficient for three-dimensional localisation. With stack-of-stars, all 32 partitions (y) for two spokes must be acquired first, before the location in the xz-plane can be determined reducing the framerate [12]. With the stack-of-stars trajectory that is used in GRASP acquisitions, for 32 partitions, 64 spokes need to be acquired to determine a 3D location whereas a 3D koosh ball sequence, potentially, only requires three spokes. This could shorten the acquisition time up to a dozen milliseconds significantly increasing the framerate. Therefore, a subsequent study could investigate the performance and framerate of a sequence with a 3D koosh ball trajectory to, hopefully, further improve 3D localisation with MRI.

It was possible to construct images that show the dynamic tracking of a GRASP sequence. The most notable difference in the images of dynamic tracked transverse line and the drawn letters is the amount of noise. The acquisition with the drawn letters shows much more noise compared to the transverse line which hardly shows any noise. This may be due to the fact that the catheter was not constantly in the phantom while drawing the letters UT. Before drawing the letter U, between the U and T and after drawing the letter T, the catheter was removed from the phantom. Since the catheter was not in the phantom, it did not give a strong signal exceeding the background noise. Thus, the radon transform identifies another, much smaller, signal peak caused by noise. This was not the case for the acquisition of the dynamic line as in this case the catheter was kept in the phantom constantly. However, since the intensity of the background noise is far lower than the intensity of the actual catheter signal setting up a threshold eliminated this noise.

This research does not feature a determination of GRASP-tracking performance in a dynamic environment. It was not possible to measure the accuracy and precision of dynamic experiments as it is not possible to run two sequences simultaneously. In order to determine dynamic tracking performance, an identical movement should be analysed for the experimental and control sequence. Subsequent studies could investigate the dynamic tracking performance through a robotic platform that guides the catheter along a predetermined path [17]. In that case, the exact same predetermined path can be tracked using both the experimental and control sequence to assess the accuracy and performance of GRASP.

5. Conclusion

Based on the results, a conclusion can be drawn on the performance of static active device tracking through a GRASP-sequence. The accuracy and precision was determined for seven positions in three-dimensional space. With average deviations situated around seven millimetres with the maximum deviation rising up to 16 millimetres in some localisations, it can be stated that the GRASP sequence, as used during this study, is not yet suitable for clinical purposes. A possible deviation in the catheter's position equal to 16 millimetres creates excessive uncertainty to guarantee successful risk-free treatment. Also, the precision that was established to be roughly three millimetres with range up to seven millimetres reaffirms that the GRASP sequence used in this research is not suitable for clinical implementation. However, it is important to keep in mind that the cause of both the relatively poor accuracy and precision is most likely due to the oscillating measurements. This refers to the sawtooth pattern visible when the individual localisations are plotted. The oscillation in the sawtooth pattern is systematic. Resolving this systematic error could greatly increase performance. Concerning the temporal resolution of GRASP tracking, it is suitable for use in 2D tracking with a frame rate that could go up to dozens of frames per second depending on the hardware but the temporal resolution does not surpass conventional 3D tracking methods that achieve up to 10 frames per second [6]. The framerate of 3D tracking is too low for clinical implementation at 1.85 frames per second. Although GRASP is capable of dynamic tracking, its clinical applicability has not been proven due to its low frame rate and the, currently, uncertain accuracy and precision. In conclusion, it can be stated that the radial golden-angle acquisition of k-space offers great opportunities in relation to active device tracking. The concept of 2D radial tracking has been proven useful in terms of temporal resolution. Also, the performance will most likely improve greatly once the systematic error is fixed allowing GRASP to become a useful sequence for future research.

References

[1] Kowalski M, Shah R, Akhrass P, Parikh V. Economics and laboratory efficiency of atrial fibrillation ablation. Curr Opin Cardiol. 2022 Jan 1;37(1):22-29. doi: 10.1097/HCO.0000000000000932.

[2] Zimetbaum P. Atrial Fibrillation. Ann Intern Med. 2017 Mar 7;166(5):ITC33-ITC48. doi: 10.7326/AITC201703070. Erratum in: Ann Intern Med. 2017 Jun 20;166(12):920.

[3] Parameswaran R, Al-Kaisey AM, Kalman JM. Catheter ablation for atrial fibrillation: current indications and evolving technologies. Nat Rev Cardiol. 2021 Mar;18(3):210-225. doi: 10.1038/s41569-020-00451-x.

[4] Wang W. Magnetic Resonance-guided Active Catheter Tracking. Magn Reson Imaging Clin N Am. 2015 Nov;23(4):579-89. doi: 10.1016/j.mric.2015.05.009.

[5] Yon, M., Delcey, M., Bour, P. et al. Continuous cardiac thermometry via simultaneous catheter tracking and undersampled radial golden angle acquisition for radiofrequency ablation monitoring. *Sci Rep* 12, 4006 (2022). doi: 10.1038/s41598-022-06927-9.

[6] Ma Y, Gogin N, Cathier P, Housden RJ, Gijsbers G, Cooklin M, O'Neill M, Gill J, Rinaldi CA, Razavi R, Rhode KS. Real-time x-ray fluoroscopy-based catheter detection and tracking for cardiac electrophysiology interventions. Med Phys. 2013 Jul;40(7):071902. doi: 10.1118/1.4808114.

[7] Campbell-Washburn AE, Tavallaei MA, Pop M, Grant EK, Chubb H, Rhode K, Wright GA. Real-time MRI guidance of cardiac interventions. J Magn Reson Imaging. 2017 Oct;46(4):935-950. doi: 10.1002/jmri.25749

[8] Active tracking - real-time MRI guided ablation [Internet]. Imricor Medical Systems; 2016 [cited 2023 Jun 22]. Available from: https://www.youtube.com/watch?v=5bnLnOx6VJc

[9] Mukherjee RK, Chubb H, Roujol S, Razavi R, O'Neill MD. Advances in Real-Time MRI-Guided Electrophysiology. Curr Cardiovasc Imaging Rep. 2019 Feb;12(2):6. doi: 10.1007/s12410-019-9481-9.

[10] Bock M, Müller S, Zuehlsdorff S, Speier P, Fink C, Hallscheidt P, Umathum R, Semmler W. Active catheter tracking using parallel MRI and real-time image reconstruction. Magn Reson Med. 2006 Jun;55(6):1454-9. doi: 10.1002/mrm.20902.

[11] Feng L, Wen Q, Huang C, Tong A, Liu F, Chandarana H. GRASP-Pro: imProving GRASP DCE-MRI through self-calibrating subspace-modeling and contrast phase automation. Magn Reson Med. 2020 Jan;83(1):94-108. doi: 10.1002/mrm.27903.

[12] Feng L. Golden-Angle Radial MRI: Basics, Advances, and Applications. J Magn Reson Imaging. 2022 Jul;56(1):45-62. doi: 10.1002/jmri.28187

[13] Block KT, Chandarana H, Milla S, Bruno M, Mulholland T, Fatterpekar G, Hagiwara M, Grimm R, Geppert C, Kiefer B, Sodickson DK. Towards Routine Clinical Use of Radial Stack-of-Stars 3D Gradient-Echo Sequences for Reducing Motion Sensitivity. J Korean Soc Magn Reson Med. 2014 Jun;18(2):87-106. doi: 10.13104/jksmrm.2014.18.2.87

[14] Baltus S. Accuracy and precision assessment on the active MR- tracking of an ablation catheter by the BEAT-sequence. 2021

[15] Lauzon ML, Rutt BK. Effects of polar sampling in k-space. Magn Reson Med. 1996 Dec;36(6):940-9. doi: 10.1002/mrm.1910360617.

[16] Daniels BR, Pratt R, Giaquinto R, Dumoulin C. Optimizing accuracy and precision of micro-coil localization in active-MR tracking. Magn Reson Imaging. 2016 Apr;34(3):289-97. doi: 10.1016/j.mri.2015.11.005.

[17] Z. Dong *et al*., "Shape Tracking and Feedback Control of Cardiac Catheter Using MRI-Guided Robotic Platform—Validation With Pulmonary Vein Isolation Simulator in MRI," in *IEEE Transactions on Robotics*, vol. 38, no. 5, pp. 2781-2798, Oct. 2022, doi: 10.1109/TRO.2022.3154691.

Appendix A – Sequence Settings

\\USER\Wyger\Active Tracking\20230607 RAVE Tracking\BEAT_interactive_1rep posA
TA: 0.3 s PM: FIX Voxel size: 2.8×2.8×10.0 mmPAT: 2 Rel. SNR: 1.00 : tfi

Properties

Prio recon	Off
Load images to viewer	On
Inline movie	Off
Auto store images	Off
Load images to stamp segments	Off
Load images to graphic segments	Off
Auto open inline display	Off
Auto close inline display	Off
Start measurement without further preparation	Off
Wait for user to start	Off
Start measurements	Single measurement

Routine

Slice group	1
Slices	1
Dist. factor	20 %
Position	L6.7 P92.1 F4.1 mm
Orientation	Coronal
Phase enc. dir.	R >> L
AutoAlign	---
Phase oversampling	0 %
FoV read	360 mm
FoV phase	100.0 %
Slice thickness	10.0 mm
TR	225.12 ms
TE	1.46 ms
Averages	1
Concatenations	1
Filter	None
Coil elements	CA

Contrast - Common

TR	225.12 ms
TE	1.46 ms
Magn. preparation	None
Flip angle	70 deg
Fat suppr.	None
Wrap-up Magn.	Restore

Contrast - Dynamic

Averages	1
Averaging mode	Short term
Reconstruction	Magnitude
Measurements	1
Multiple series	Off

Resolution - Common

FoV read	360 mm
FoV phase	100.0 %
Slice thickness	10.0 mm
Base resolution	128
Phase resolution	75 %
Phase partial Fourier	Off
Trajectory	Cartesian
Interpolation	Off

Resolution - iPAT

PAT mode	GRAPPA
Accel. factor PE	2

Resolution - iPAT

Ref. lines PE	24
Reference scan mode	Integrated

Resolution - Filter Image

Image Filter	Off
Distortion Corr.	Off
Prescan Normalize	Off
Normalize	Off
B1 filter	Off

Resolution - Filter Rawdata

Raw filter	Off
Elliptical filter	Off

Geometry - Common

Slice group	1
Slices	1
Dist. factor	20 %
Position	L6.7 P92.1 F4.1 mm
Orientation	Coronal
Phase enc. dir.	R >> L
FoV read	360 mm
FoV phase	100.0 %
Slice thickness	10.0 mm
TR	225.12 ms
Multi-slice mode	Sequential
Series	Ascending
Concatenations	1

Geometry - AutoAlign

Slice group	1
Position	L6.7 P92.1 F4.1 mm
Orientation	Coronal
Phase enc. dir.	R >> L
AutoAlign	---
Initial Position	L6.7 P92.1 F4.1
L	6.7 mm
P	92.1 mm
F	4.1 mm
Initial Rotation	0.00 deg
Initial Orientation	Coronal

Geometry - Saturation

Fat suppr.	None
Wrap-up Magn.	Restore
Special sat.	None

Geometry - Navigator

System - Miscellaneous

Positioning mode	FIX
Table position	H
Table position	0 mm
MSMA	S - C - T
Sagittal	R >> L
Coronal	A >> P
Transversal	F >> H
Coil Combine Mode	Adaptive Combine
Save uncombined	Off
Matrix Optimization	Off

System - Miscellaneous

AutoAlign	---
Coil Select Mode	Default

System - Adjustments

B0 Shim mode	Tune up
Adjust with body coil	Off
Confirm freq. adjustment	Off
Assume Dominant Fat	Off
Assume Silicone	Off
Adjustment Tolerance	Auto

System - Adjust Volume

Position	Isocenter
Orientation	Transversal
Rotation	0.00 deg
A >> P	263 mm
R >> L	350 mm
F >> H	350 mm
Reset	Off

System - Tx/Rx

Frequency 1H	63.641556 MHz
Correction factor	1
Gain	High
Img. Scale Cor.	1.000
Reset	Off
? Ref. amplitude 1H	0.000 V

Physio - Signal1

1st Signal/Mode	None
TR	225.12 ms
Concatenations	1
Segments	60

Physio - Cardiac

Magn. preparation	None
Fat suppr.	None
Dark blood	Off
FoV read	360 mm
FoV phase	100.0 %
Phase resolution	75 %
Cine	Off
Trajectory	Cartesian

Physio - PACE

Resp. control	Off
Concatenations	1

Sequence - Part 1

Introduction	Off
Dimension	2D
Reordering	Linear
Asymmetric echo	Off
Contrasts	1
Optimization	Min. TE TR
Multi-slice mode	Sequential
Echo spacing	2.9 ms
Sequence type	Trufi
Bandwidth	1002 Hz/Px

Sequence - Part 2

Define	Shots
Shots per slice	1

Sequence - Part 2

Segments	60
Trufi delta freq.	0 Hz
RF pulse type	Normal
Gradient mode	Fast
Excitation	Slice-sel.
Flip angle mode	Constant
Cine	Off

Sequence - Interactive

Tracking	On
Slice Following	ON + SG1
Slice Following Mode	Tip Tracking
Slice Following Sens.	1 mm
Background Suppr.	1 mT/m
Tracking Flip Angle	7 deg
Pause	Off
Acquisition Order	1
Mosaic	Off

Sequence - Assistant

Mode	Off
Allowed delay	0 s

\\USER\Wyger\Active Tracking\20230607 RAVE Tracking\RAVE 256v posA
TA: 0:42 PM: FIX Voxel size: 2.5×2.5×2.5 mmRel. SNR: 1.00 : RAVE

Properties

Prio recon	Off
Load images to viewer	On
Inline movie	Off
Auto store images	On
Load images to stamp segments	Off
Load images to graphic segments	Off
Auto open inline display	Off
Auto close inline display	Off
Start measurement without further preparation	Off
Wait for user to start	Off
Start measurements	Single measurement

Routine

Slab group	1
Slabs	1
Dist. factor	20 %
Position	L0.7 P3.7 F2.9 mm
Orientation	Coronal
Phase enc. dir.	R >> L
AutoAlign	---
Slice oversampling	0.0 %
Slices per slab	32
FoV read	320 mm
FoV phase	100.0 %
Slice thickness	2.50 mm
TR	5.00 ms
TE	2.50 ms
Filter	None
Coil elements	CA;SP1-3

Contrast - Common

TR	5.00 ms
TE	2.50 ms
Flip angle	5 deg
Fat suppr.	None

Contrast - Dynamic

Reconstruction	Magnitude
Measurements	1
Multiple series	Off

Resolution - Common

FoV read	320 mm
FoV phase	100.0 %
Slice thickness	2.50 mm
Base resolution	128
Radial views	256
Slice resolution	100 %
Slice partial Fourier	Off
Trajectory	Radial
Interpolation	Off

Resolution - Filter Image

Image Filter	Off
Distortion Corr.	Off
Prescan Normalize	Off
Normalize	Off
B1 filter	Off

Resolution - Filter Rawdata

Raw filter	Off
Elliptical filter	Off

Geometry - Common

Slab group	1
Slabs	1
Dist. factor	20 %
Position	L0.7 P3.7 F2.9 mm
Orientation	Coronal
Phase enc. dir.	R >> L
Slice oversampling	0.0 %
Slices per slab	32
FoV read	320 mm
FoV phase	100.0 %
Slice thickness	2.50 mm
TR	5.00 ms
Multi-slice mode	Sequential
Series	Ascending

Geometry - AutoAlign

Slab group	1
Position	L0.7 P3.7 F2.9 mm
Orientation	Coronal
Phase enc. dir.	R >> L
AutoAlign	---
Initial Position	L0.7 P3.7 F2.9
L	0.7 mm
P	3.7 mm
F	2.9 mm
Initial Rotation	0.00 deg
Initial Orientation	Coronal

Geometry - Saturation

Fat suppr.	None
Special sat.	None

System - Miscellaneous

Positioning mode	FIX
Table position	H
Table position	0 mm
MSMA	S - C - T
Sagittal	R >> L
Coronal	A >> P
Transversal	F >> H
Coil Combine Mode	Sum of Squares
Save uncombined	Off
Matrix Optimization	Off
Coil Focus	Flat
AutoAlign	---
Coil Select Mode	On - AutoCoilSelect

System - Adjustments

B0 Shim mode	Tune up
Adjust with body coil	Off
Confirm freq. adjustment	Off
Assume Dominant Fat	Off
Assume Silicone	Off
Adjustment Tolerance	Auto

System - Adjust Volume

Position	Isocenter
Orientation	Transversal
Rotation	0.00 deg
A >> P	263 mm
R >> L	350 mm
F >> H	350 mm
Reset	Off

System - Tx/Rx

Frequency 1H	63.641556 MHz
Correction factor	1
Gain	Low
Img. Scale Cor.	1.000
Reset	Off
? Ref. amplitude 1H	0.000 V

Inline - Common

Subtract	Off
Measurements	1
StdDev	Off
Save original images	On

Inline - MIP

MIP-Sag	Off
MIP-Cor	Off
MIP-Tra	Off
MIP-Time	Off
Save original images	On

Inline - Composing

Distortion Corr.	Off

Sequence - Part 1

Introduction	Off
Dimension	3D
Contrasts	1
Multi-slice mode	Sequential
Bandwidth	500 Hz/Px

Sequence - Part 2

Gradient mode	Fast
RF spoiling	On

Sequence - Special

Profile order	Golden Angle
Partition order	Centric
ICE gradient calibration	Off
FFT Scaling	1.00

Sequence - Assistant

Mode	Off